



# Stress Corrosion Cracking Behavior of Alloy 718 Subjected to Various Thermal Mechanical Treatments in Primary Water

Mi Wang, Miao Song, Gary S. Was and L. Nelson

**Abstract** Alloy 718 is an age hardenable, nickel-base alloy used in fuel assembly of Pressurized Water Reactors (PWRs) by virtue of its high strength and resistance to corrosion and stress corrosion cracking (SCC). SCC susceptibility is affected by the microstructure developed during thermal mechanical treatments. The SCC behavior of alloy 718 in three different thermal mechanical treatments (TMTs) and two different heats was studied in PWR primary water environment using constant extension rate tensile (CERT) tests. TMTs have a significant effect on the microstructure and thus the mechanical behavior and the SCC susceptibility of alloy 718. TMTs using a solution anneal at 1093 °C with a two-step ageing treatment (1093 °C/1 h + 718 °C/8 h + 621 °C/8 h) exhibited the best SCC resistance.

**Keywords** Alloy 718 · Stress corrosion cracking · Microstructure · Mechanical properties · Primary water

## Introduction

Stress corrosion cracking (SCC) of high strength components such as fasteners and springs are significant problems in PWRs. Alloy 718, used as structural material in PWRs, is a precipitation hardened, nickel-base alloy, known for its excellent mechanical properties [1, 2], good corrosion resistance [3] and relative ease of manufacturing. The SCC behavior of alloy 718 depends heavily on the heat treatment [4–10]. The traditional heat treatments produce precipitates at the grain boundaries that were very beneficial in minimizing high-temperature creep [11], but are not necessarily beneficial for SCC resistance in a PWR primary water environment. Modified heat treatments, also known as modified grades, were developed specif-

---

M. Wang (✉) · M. Song · G.S. Was  
University of Michigan, 48109 Ann Arbor, MI, USA  
e-mail: miwan@umich.edu

L. Nelson  
JLN Consulting, Mills River, NC 28759, USA

ically for nuclear applications that may provide SCC initiation resistance, but have relatively high crack propagation rates [10]. However, little SCC data exists on these different modified heat treatments.

The microstructure of alloy 718 is also highly dependent on the heat treatment schedule, which can consist of multiple steps. The primary strengthening precipitate in alloy 718 is  $DO_{22}$ -ordered  $Ni_3$  (Nb, Ti, Al) ( $\gamma''$  phase) although the  $L1_2$ -ordered  $Ni_3$  (Ti, Al, Nb) ( $\gamma'$  phase) also contributes to the alloy's strength to a certain extent. Other phases such as  $Ni_3Nb$  ( $\delta$ -phase), Laves phase and MC carbide may also be present. Laves phase has been shown to have a detrimental effect on room temperature and high temperature (649 °C) mechanical properties [4, 12]. Thus, recent heat treatments of alloy 718 have been modified to avoid the presence of Laves phase. This paper examines alloy 718 with three different thermal mechanical treatments and two heats, and their effect on mechanical properties and stress corrosion cracking susceptibility in PWR primary water environment.

## Experimental

### *Materials and Samples Design*

Two heats and three thermal mechanical treatments of alloy 718 were used in this study. The chemical compositions are given in Table 1. There is a very slight difference in the major elements between the normal and optimized conditions. The three different TMTs are described in Table 2 and can be divided into three groups based on the solution annealing temperature and the aging steps:

- *Group I* solution annealed at 1093 °C for 1 h followed by water quenching, then aging at 718 °C for 8 h, cooled at 55 °C/h to 621 °C and aged for another 8 h, then air cooled to room temperature.
- *Group II* solution annealed at 945 °C for 1 h followed by water quenching, intermediate cold worked to 10%, then aging at 718 °C for 8 h, cooled at 55 °C/h to 621 °C and aged for 8 h, then air cooled to room temperature.
- *Group III* solution annealed at 1065 °C for 0.5 h followed by water quenching, intermediate cold worked to 10%, then aging at 760 °C for 10 h, cooled at 55 °C/h to 649 °C and aged for 20 h, then air cooled to room temperature.

The tensile samples have a square gage section of 2 mm, a gage length of 21 mm and threaded ends, as shown in Fig. 1. Before using in any experiments, all the samples were mechanically polished with silicon carbide abrasive paper from 360 to 4000 grit then electropolished (10 vol.% perchloric acid in methanol solution at -40 °C at a voltage around 30 V for 30 s) to obtain a mirror finish. A 2100F JEOL Transmission Electron Microscopy (TEM) was used to characterize the microstructure with all experimental conditions detailed elsewhere [13].

**Table 1** Chemical compositions of alloy 718 (wt%)

Heat No.	Condition	Ni	Cr	Fe	Nb	Mo	Ti	Al	Ta	C	Si	Mn	Co	P	Cu	S
011399	Normal	52.77	18.46	18.95	5.2	2.9	0.96	0.61	0.01	0.036	0.02	0.01	0.01	0.005	0.01	0.0005
011400	Optimized	52.73	18.49	19.18	5.01	2.9	0.76	0.78	0.02	0.036	0.02	0.01	0.01	0.005	0.01	0.0005

**Table 2** Different thermal mechanical treatments (TMTs) of alloy 718

Group	Condition	Thermal mechanical treatments (TMTs) <sup>a</sup>
I	718A	1093/1 + 0% + 718/8 + 621/8
	718A(O)	1093/1 + 0% + 718/8 + 621/8
II	718B	945/1 + 10% + 718/8 + 621/8
	718B(O)	945/1 + 10% + 718/8 + 621/8
III	718C	1065/0.5 + 10% + 760/10 + 649/30

<sup>a</sup>Temperature (°C)/Time(h) + Cold Work (%) + Temperature (°C)/Time(h) (O) = Optimized heat

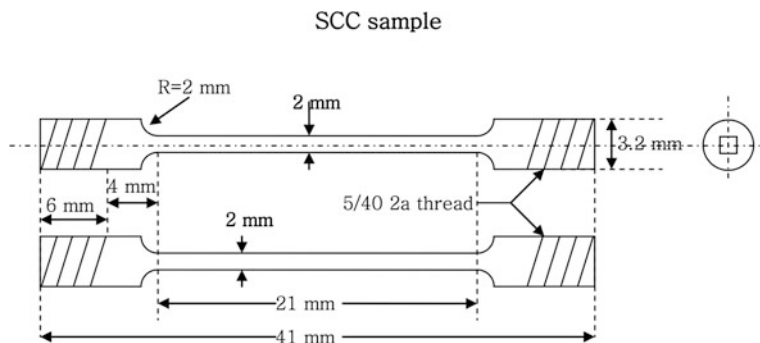


**Fig. 1** Schematic diagram of tensile sample

### ***Mechanical Properties Test Conditions***

Microhardness and tensile tests at room temperature were used to study the mechanical properties. Microhardness was measured using a Vickers Hardness indenter (Buehler MICROMET II Hardness Tester) with a load of 1000 g. Tensile tests at room temperature were performed using an MTS Machine (TR/50) and extensometer (MTS 634.12F-24). The tensile tests were conducted at a strain rate of  $1 \times 10^{-4} \text{ s}^{-1}$  to failure at room temperature.

### ***CERT Test and Crack Characterization***

The CERT experiments were conducted in a 4 L stainless steel autoclave that was connected to a flowing water loop fed from an external water column in which the addition of gas was made. It is capable of straining four samples in parallel providing identical conditions within a given test. CERT experiments were conducted at a strain rate of  $1 \times 10^{-7} \text{ s}^{-1}$  in PWR primary water environment (320 °C, 2000 psi, 35 cc/kg dissolved hydrogen, 1000 ppm [B] and 2 ppm [Li]) to 4–6% plastic strain. The conductivity, oxygen content, hydrogen content, and B, and Li

concentrations were chosen to be representative of water chemistry in a PWR core. After the CERT test, the gage section of each tensile sample (about 1 mm<sup>2</sup> area) was characterized in an SEM (JEOL JSM-6480) to determine the surface morphology and cracking susceptibility.

## Results

### *Microstructure and Mechanical Properties of Alloy 718*

Microstructural features, including grain size, and precipitation ( $\gamma'$  +  $\gamma''$  phases) were characterized for all the conditions. Figure 2 shows the microstructure of selected conditions 718A, 718B, and 718C. 718A was not cold worked which consisted of grains with well-defined grain boundaries. Slight surface deformation due to the cold work was observed on 718B and 718C, grain boundaries were less well-defined. The grain sizes of the various alloy 718 conditions are listed in Table 3. The grain size was estimated based on the linear interception method. Group II had the smallest average grain size around 6  $\mu\text{m}$  while Group I and III had relatively large grain sizes, mostly was around 100–150  $\mu\text{m}$ . The optimized heat materials generally had a coarser grain size than the normal heat at the same heat treatment condition.

Detailed microstructural characterization of the conditions was conducted by Silva et al. [13], including TEM characterization of  $\gamma'$  and  $\gamma''$ -phase precipitates. The average diameters together with the number densities of the precipitates are summarized in Table 3. The average diameter of precipitates in Group II was about 10 nm and about 17 nm in Group III. The precipitates sizes and densities of Group I were both lower than those of Group II. Thus, the volume fraction of the precipitates was the lowest in Group I. On the other hand, the presence of  $\delta$ -phase and the significant difference in this phase among the TMTs was also observed, as shown in Fig. 2. The bright-contrast particles with particular shape, such as platelet- or needle-like shape, were only be observed in Fig. 2b, but not in the other two conditions (Fig. 2a, c). Previous EDX analysis proved that this type of particles were mainly consisted of Ni and Nb with small amount of Ti [13]. Together with

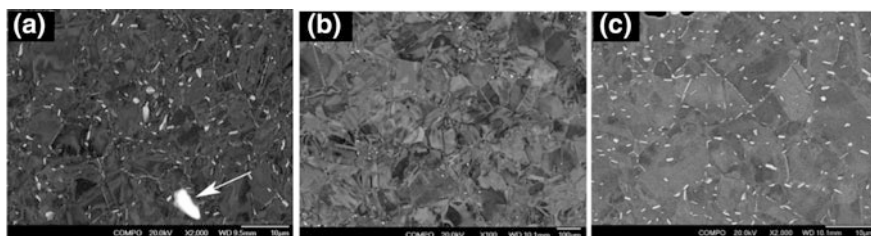


**Fig. 2** SEM micrographs of samples: **a** 718A, **b** 718B, and **c** 718C [13]

**Table 3** Microstructural characterization [13] and hardness measurements of alloy 718 in different conditions

Group	Condition	Grain size ( $\mu\text{m}$ )	Size (nm)	$\gamma' + \gamma''$ phases density ( $10^{22}/\text{m}^3$ )	Volume fraction (%)	Hardness (Hv)
I	718A	$114 \pm 9$	$6.6 \pm 1.4$	3.99	0.6	$447 \pm 16$
	718A(O)	$143 \pm 16$	$5.0 \pm 1.6$	3.31	0.2	$378 \pm 12$
II	718B	$6 \pm 0.2$	$10.0 \pm 3.4$	4.95	2.6	$492 \pm 10$
	718B(O)	$13 \pm 1$	NM	NM	NM	$460 \pm 15$
III	718C	$93 \pm 6$	$27.4 \pm 8.0$	0.18	1.9	$463 \pm 16$

(O) Optimized heat, NM no measurement

the particle morphology, it should be considered as the  $\delta$ -phase ( $\text{Ni}_3\text{Nb}$ ). There was a high amount of  $\delta$ -phase in Group II conditions, both at the grain boundary and inside of grain, while the presence of  $\delta$ -phase was difficult to confirm in the other conditions. Nevertheless, there was not a reliable method of quantifying this phase. The large amount of  $\delta$ -phase at the grain boundaries in Group II can pin the grain boundaries and inhibit grain growth, which may be responsible for the small grain size of Group II samples.

As a precipitate-strengthened nickel-base alloy, the Vickers microhardness of alloy 718 was also quite high in the as-received condition, Table 3. Group II showed the highest hardness among all conditions and the other groups showed similar hardness.

Tensile test results of alloy 718 with different conditions are plotted in Fig. 3. They were tested in the as-received conditions and the mechanical properties data are tabulated in Table 4. All alloys showed high strength, consistent with the literature [10]. Among the TMTs studied, Group II showed the highest yield stress and ultimate tensile stress. Group I showed relatively low stress levels, Group III was higher than Group I, but lower than Group II.

### Cracking Behavior in PWR Primary Water

Cracking characterization for each condition includes the following parameters:

- average crack length;
- crack density: the number of crack observed per unit area;
- crack length per unit area: the total crack length divided by the analyzed area.

The criterion used for evaluating the cracking behavior is the crack length per unit area, because it combines both average crack length and crack density, and is therefore more representative of the cracking behavior.

Intergranular cracks were observed in all the TMT conditions. Examples of cracks are shown in Fig. 4 in which the stress was in the horizontal direction. Most

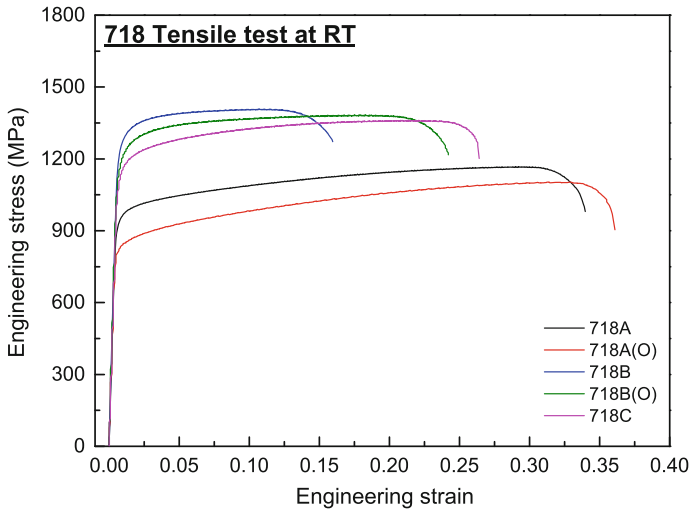


**Fig. 3** Stress–strain curve for various conditions of as-received alloy 718 at room temperature in air

**Table 4** Mechanical properties of alloy 718 in different conditions at room temperature

Group	Condition	Elastic modulus (GPa)	Yield stress (MPa)	Ultimate tensile stress (MPa)	Plastic strain at UTS (%)
I	718A	194.5	927	1168	33
	718A(O)	194.7	815	1104	32.1
II	718B	212.2	1234	1409	15
	718B(O)	219.3	1183	1383	17.9
III	718C	219.9	1030	1310	25.3

(O) Optimized heat

cracks were clearly visible and were either narrow or wide open depending on the TMT. The cracks for 718B(O) condition were fairly short and thus highlighted in dashed yellow circles. The average crack length, crack density, and crack length per unit area are listed in Table 5, together with the CERT results in PWR primary water environment. The crack length per unit area of all tested conditions is plotted in Fig. 5.

It was clear that Group I TMTs (A, and A(O)) were less susceptible to SCC in primary water environment than the other groups. Groups II and III all had high susceptibility to SCC in primary water. The average crack length was more or less related to the grain size of each condition. For example, Group II conditions (B, and B(O)) had the smallest grain sizes, thus the average crack lengths were also the smallest. However, it also had extremely high crack density resulting in the highest cracking susceptibility among all the conditions.

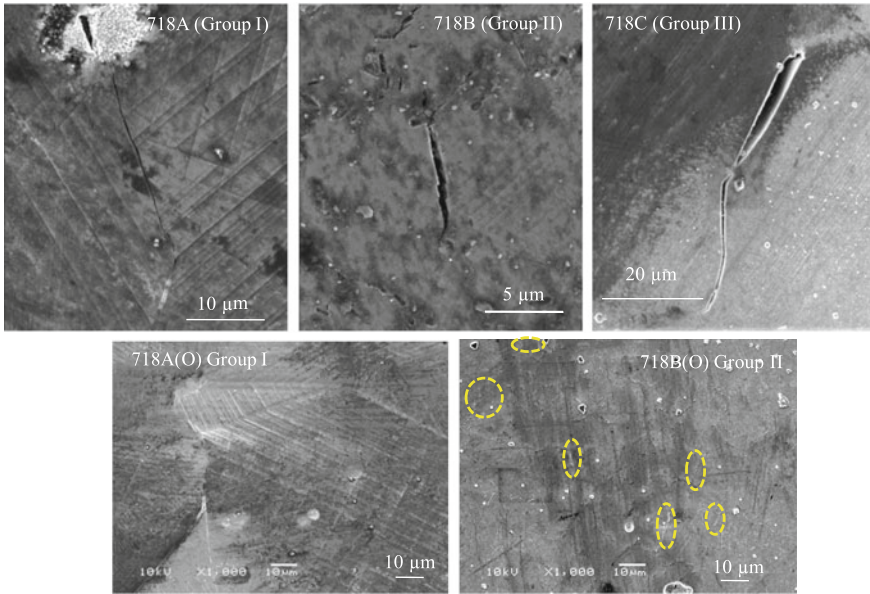


**Fig. 4** SEM micrographs of 718 with Groups I (718A and A(O)), II (718B and B(O)), III (718C), TMTs and strained to 4–6% in PWR primary water environment (stress is in the horizontal direction)

**Table 5** CERT test results and the corresponding cracking data of alloy 718 strained to 4–6% in PWR primary water environment

Group	Condition	Yield stress (MPa)	Plastic strain (%)	Average crack length ( $\mu\text{m}$ )	Crack density (#cracks/ $\text{mm}^2$ )	Crack length per unit area ( $\mu\text{m}/\text{mm}^2$ )
I	718A	$870 \pm 8$	$5.15 \pm 0.1$	$16 \pm 2$	$38 \pm 0.2$	$609 \pm 84$
	718A(O)	$733 \pm 16$	$5.95 \pm 0.03$	$14 \pm 2$	$42 \pm 0.3$	$569 \pm 78$
II	718B	$1176 \pm 13$	$3.25 \pm 0.03$	$4 \pm 0.2$	$222 \pm 1$	$930 \pm 55$
	718B(O)	$1115 \pm 24$	$3.8 \pm 0.04$	$5 \pm 0.2$	$794 \pm 5$	$4073 \pm 149$
III	718C	$966 \pm 15$	$4.6 \pm 0.04$	$11 \pm 1$	$99 \pm 1$	$1125 \pm 107$

(O) Optimized heat

## Discussion

### *Microstructure Evolution with Chemical Composition*

The major difference between the chemical compositions of the two heats was in the amount of Nb, Ti, and Al. These three elements are important for precipitation behavior of alloy 718. Table 6 shows the sum of (Al + Ti + Nb) in at.% and ratio



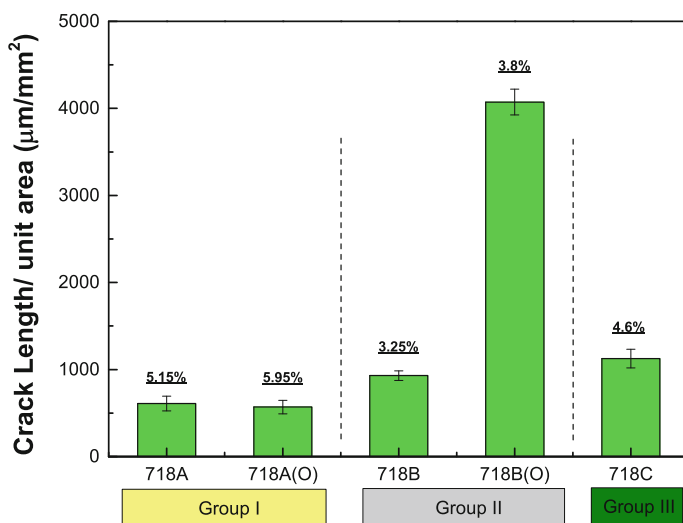


**Fig. 5** Cracking susceptibility of alloy 718 with different TMTs following straining to 4–6% in PWR primary water environment

between (Al + Ti) and Nb in at.% for normal and optimized conditions. This value can help to determine the volume fraction of precipitates. Thus, the high temperature yield stress and ultimate stress were highly dependent on the sum of (Al + Ti + Nb) at.% as suggested by Ref. [14]. The increase (Al + Ti + Nb) at.% may result in a higher strength. More important, the ratio of (Al + Ti)/Nb can be used to predict the relative volume fraction of  $\gamma'$  and  $\gamma''$  phases due to the fact that Al and Ti are  $\gamma'$  stabilizer while Nb is more predominant in  $\gamma''$  phase [15]. The increase in (Al + Ti)/Nb ratio favor  $\gamma'$  rather than  $\gamma''$  precipitation. 718A and 718A(O), 718B and 718B(O) shared the same TMTs respectively but had different chemical compositions. Conditions 718A and 718B had higher yield stress and tensile stress (Table 4) and they also had a higher (Al + Ti + Nb) at.% and a lower (Al + Ti)/Nb ratio, than 718A(O) and 718B(O). The volume fraction of ( $\gamma'$  +  $\gamma''$ ) phases reported for the normal and the optimized heats were quite close to each other [13]. Indeed, more  $\gamma'$  precipitation strengthening effect might be applied to the optimized (O) heat; however,  $\gamma''$  is the one usually considered as the primary strengthening precipitate. This may explain the lower mechanical properties for the optimized heat.

### *Effect of Microstructure on SCC Susceptibility*

In an attempt to explain the difference on the basis of the microstructure, Fig. 6 illustrates the relationship between the SCC susceptibility of alloy 718 in primary

**Table 6** (Al + Ti + Nb) content and (Al + Ti)/Nb ratio in at.% of normal and optimized heats

Condition	(Al + Ti + Nb) in at. %	(Al + Ti)/Nb in at. %
Normal	5.707	0.762
Optimized	5.698	0.831

water and the different microstructural features: grain size, ( $\gamma' + \gamma''$ ) phases. It was difficult to identify a pattern or correlation which can link the cracking behavior with any of these features. The grain size might have a slight influence. As shown in Fig. 6a, except for 718B, smaller grain size had higher cracking frequency than the larger grain conditions. The reason that 718B did not fit this pattern might due to relatively low plastic strain ( $\sim 3\%$ ) compared to the other samples (5–6%). The observation from SCC susceptibility (Fig. 5) was that the Group II conditions had the worst SCC behavior while the Group I conditions had the best. Other than grain size, the most significant difference between Group II microstructure compared to that for the other groups was the large amount of  $\delta$ -phase at the grain boundaries and also in the grains. It was reported that conditions with grain boundaries free of  $\delta$ -phase were more resistant to SCC than the ones with grain boundaries decorated with  $\delta$ -phase [16, 17]. As noted by Sheth et al. [18] the SCC growth rate values were observed to scale with the qualitative amount of  $\delta$ -phase found at the grain boundaries. But the lack of a proper method for quantifying the  $\delta$ -phase in all conditions made neither the interpretation nor the correlation possible at this stage. Lastly, the relationship between the cracking susceptibility in primary water and the mechanical properties is plotted in Fig. 7. The grain size and yield strength vary inversely with each other as expected. A bounding curve was applied to the SCC dependence on yield strength of alloy 718. It fit well with all but the 718B point,

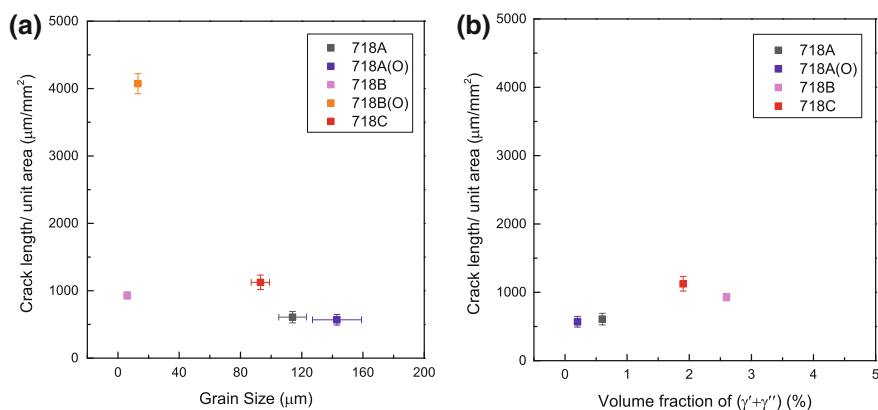
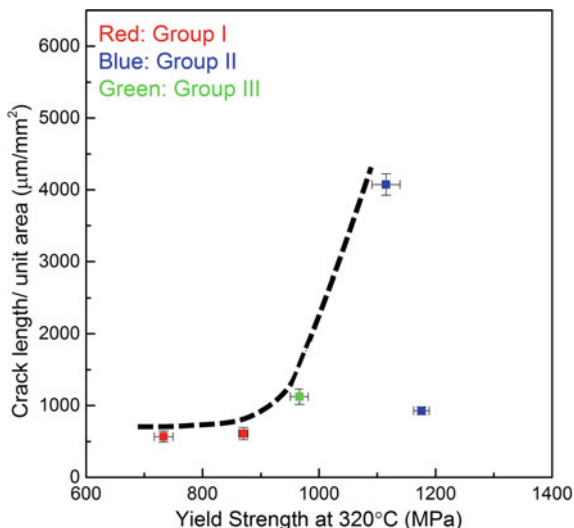


**Fig. 6** Relationship between SCC behavior in primary water and microstructural features: **a** grain size and **b** volume fraction of ( $\gamma' + \gamma''$ ) phases

**Fig. 7** Relationship between SCC behavior in primary water and yield stress at 320 °C, black dash line is bounding curve via visual guide



similar to the case of grain size shown in Fig. 6a. However, this bounding curve cannot be easily correlated with the microstructural features as discussed in the previous paragraph.

## Conclusion

The SCC susceptibility of alloy 718 was evaluated for three thermo-mechanical treatments and two heats. The chemical composition and thermo-mechanical treatment showed significant impact on the microstructure for the as-received materials. Alloy 718 solution annealed at 945 °C and followed by a two-step aging treatment showed the highest yield stress and hardness, but the poorest SCC resistance, while a solution anneal at 1093 °C followed by a two-step ageing treatment showed the lowest yield stress, but the best SCC resistance. The optimized heat treatment resulted in a lower yield strength compared to that for the normal heat treatments. A bounding curve between cracking susceptibility and yield stress indicated a rough correlation between SCC susceptibility and yield strength. However, microstructural features such as grain size and ( $\gamma'$  +  $\gamma''$ ) precipitation cannot explain the SCC susceptibility of alloy 718 in primary water. In summary, alloy 718 with a TMT consisting of 1093 °C/1 h + 718 °C/8 h + 621 °C/8 h had very low SCC susceptibility in PWR primary water. Moreover, the consistency of SCC behavior of this TMT regardless of the heat-to-heat variability makes it more reliable in performance stability. It should be considered as a potential treatment for alloy 718 structural applications in current and next generation nuclear reactors.

**Acknowledgements** Support for this work was provided by the Electric Power Research Institute (contract no: MA10001593). The authors gratefully acknowledge the facilities provided by the High Temperature Corrosion Laboratory at the University of Michigan. The authors would also like to thank Dr. Chinthaka Silva from the Oak Ridge National Laboratory for the microstructural characterization.

## References

1. Technical report: materials handbook for nuclear pressure boundary application. EPRI, Palo Alto, CA. 3002000122 (2013)
2. Y. Katayama et al., SCC properties of modified Alloy 718 in BWR plant, in *Proceeding of the 15th International Symposium on Environmental Degradation of Materials in Nuclear Power Systems—Water Reactors*, Colorado Spring, CO. The Minerals, Metals and Materials Society, Warrendale, PA, pp. 763–776 (2011)
3. Technical report: inconel Alloy 718. INCO alloys international bulletin, Huntington Alloys Corporation, 3200 Riverside Drive, Huntington, WV (1978)
4. M.B. Burke, Technical report: microstructural characterization of Alloy 718. EPRI, Palo Alto, CA, TR-103970 (1994)
5. D. Alter, P. Dewes, F. Garzarolli, Technical report: influence of irradiation and stress/strain on the behavior of structural materials, Phase 1. EPRI, Palo Alto, CA, NP-7533M (1991)
6. P. Dewes, R. Hahn, D. Alter, F. Garzarolli, Technical report: influence of irradiation and stress/strain on the behavior of structural materials, Phase 2. EPRI, Palo Alto, CA, TR-107699 (1997)
7. P. Dewes, R. Hahn, D. Alter, F. Garzarolli, Technical report: influence of irradiation and stress/strain on the behavior of structural materials, Phase 3. EPRI, Palo Alto, CA, TR-107670 (1997)
8. J.A. Manriquez, N.K. Sheth, J.M. Sanchez, Technical report: precipitation kinetics, thermal stability, and corrosion properties of alloy 718 and 718-based superalloys. EPRI, Palo Alto, CA, TR-103971 (1995)
9. M.T. Miglin, Technical report: improvement of the stress corrosion resistance of alloy 718 in the PWR environment. EPRI, Palo Alto, CA, TR-105808 (1996)
10. J. Nelson, Technical report: Alloy 718 review for fuel assembly application. EPRI, Palo Alto, CA, 3002002176 (2013)
11. K. Sadananda, P. Shahinian, Creep crack growth in alloy 718. *Metall. Trans. A* **8A**, 439–449 (1977)
12. I.L.W. Wilson, M.B. Burke, The effect of microstructure on the SCC behavior of alloy 718, in *Superalloys 718, 625 and Various Derivatives*, ed. by E.A. Loria (The Minerals, Metals and Materials Society, 1991), pp. 681–693
13. C. Silva et al., Characterization of alloy 718 subjected to different thermomechanical treatments. *Mater. Sci. Eng., A* **691**, 195–202 (2017)
14. X. Xie et al., The effect of Nb, Ti, Al on precipitation and strengthening behavior of 718 type superalloys, in *Superalloys 718, 625, 706 and Various Derivatives*, ed. by E.A. Loria (The Minerals, Metals and Materials Society, 2005)
15. R. Cozar et al., Morphology of  $\gamma'$  and  $\gamma''$  precipitates and thermal stability of inconel 718 type alloys. *Metall. Trans.* **4**, 47–59 (1972)
16. M.T. Miglin, J.V. Monter, C.S. Wade, Stress corrosion of chemistry and heat treat variants of alloy 718, part 1: stress corrosion test results, in *Proceeding of 6th International Symposium on Environmental Degradation of Materials in Nuclear Power Systems—Water Reactors*, San Diego, CA. The Minerals, Metals and Materials Society, Warrendale, PA, pp. 815–819 (1993)

17. M.T. Miglin, T.R. Mager, J.L. Nelson, Stress corrosion of chemistry variants of alloy 718, part 2: microstructural characterization, in *Proceeding of 6th International Symposium on Environmental Degradation of Materials in Nuclear Power Systems—Water Reactors*, San Diego, CA. The Minerals, Metals and Materials Society, Warrendale, PA, pp. 821–827 (1993)
18. N.K. Sheth et al., Delta ( $\text{Ni}_3\text{Nb}$ ) and IGSCC degradation in alloy 718 and derivatives, in *Proceeding of 6th International Symposium on Environmental Degradation of Materials in Nuclear Power Systems—Water Reactors*, San Diego, CA. The Minerals, Metals and Materials Society, Warrendale, PA, pp. 829–835 (1993)